DOI: 10.1002/ejic.200501078

# Multielectron Storage and Photo-Induced Electron Transfer in Oligonuclear Complexes Containing Ruthenium(II) Terpyridine and Ferrocene Building Blocks

**Katja Heinze,*[a] Klaus Hempel,[a] and Manuela Beckmann[a]**

**Keywords:** Electron transfer / Heterometallic complexes / Luminescence / Metallocenes / Ruthenium

The heteroleptic complex $[(HOOC\text{-}tpy)Ru(tpy\text{-}NH_2)](PF_6)_2$ (tpy = 2,2′;6′,2′′-terpyridine) has been incorporated into a multicomponent system with ferrocene moieties attached on either the N-terminal end or the C-terminal end and on both ends of the ruthenium complex. Electrochemical studies reveal almost noninteracting subunits in the oligonuclear systems, whereas ground-state and excited-state optical properties are shown to strongly depend on the site of ferrocene attachment. Interpretation of the experimental results is supported by DFT calculations.


## Introduction

Design and synthesis of multicomponent systems such as polynuclear metal complexes incorporating electroactive and/or photoactive moieties, especially ruthenium polypyridine complexes,[1–11] is of great current interest for fundamental studies of energy and electron transfer and photoinduced charge separation modelling natural photosynthesis[12] as well as in terms of potential applications in molecular wires and devices, photocatalysis, energy conversion and information storage.[13–17] Most of these topics rely fundamentally on vectorial energy or electron transfer that requires asymmetric multicomponent systems. This requirement has been elegantly met by the design of metallostars and metallodendrimers.[18,19]

Natural proteins represent an archetype for directional multicomponent systems with a well-defined sequence of building blocks. Biological peptides and proteins already provide interesting functions such as molecular recognition and catalysis,[20,21] while artificial amino acid building blocks expand the diversity of peptides and proteins. Combining metal-containing electroactive and photoactive units in peptide-like structures should merge the advantages of both worlds: the amide linkage provides directionality and the introduction of metal complexes provides functionality.[22–31]

In this contribution the synthesis of a bis(terpyridine) ruthenium complex with amino and carboxylato substituents and its conjugates with ferrocene units attached on the N or C terminus as well as on both ends is reported. The influence of the site of ferrocene attachment on ground- and excited-state properties of the multicomponent systems is investigated.

[a] Anorganisch-Chemisches Institut der Universität Heidelberg, Im Neuenheimer Feld 270, 69120 Heidelberg, Germany
Fax: +49-6221-545707
E-mail: katja.heinze@urz.uni-heidelberg.de
Supporting information for this article is available on the WWW under http://www.eurjic.org or from the author.

## Results and Discussion

### Design and Synthetic Strategy

The assembly of ruthenium and ferrocene building blocks is based on a modular approach using peptide chemistry.[22–24,32] The key building block is the heteroleptic complex $\mathbf{2}(PF_6)_2$ with a bis(terpyridine) ruthenium(II) core. This asymmetrical complex can be functionalised on either the C-terminal or the N-terminal end giving access to asymmetric multinuclear complexes with a well-defined sequence of building blocks.

Two synthetic challenges have to be met for the success of the synthetic strategy: (i) the selective formation of the heteroleptic complex $\mathbf{2}(PF_6)_2$ and (ii) the activation of the unreactive amino group of the positively charged complex for amide formation. The synthetic approach to $\mathbf{2}(PF_6)_2$ is outlined in Scheme 1.

The terpyridine ligands tpy-COOEt and tpy-$NH_2$ were prepared using Stille coupling reactions according to literature procedures.[33–35] To selectively obtain the heteroleptic complex $\mathbf{1}(PF_6)_2$ the ester-substituted terpyridine ligand is coordinated to ruthenium trichloride[34] before the amino-substituted terpyridine is attached using microwave irradiation (Scheme 1). This optimised procedure results in a negligible amount of homoleptic complexes and $\mathbf{1}(PF_6)_2$ was isolated in 85% yield. In the $^1H$ NMR spectrum of $\mathbf{1}(PF_6)_2$ characteristic singlet signals for the protons $H^2$ and $H^{2'}$ are observed at $\delta$ = 9.15 and $\delta$ = 7.96, respectively, while the

  

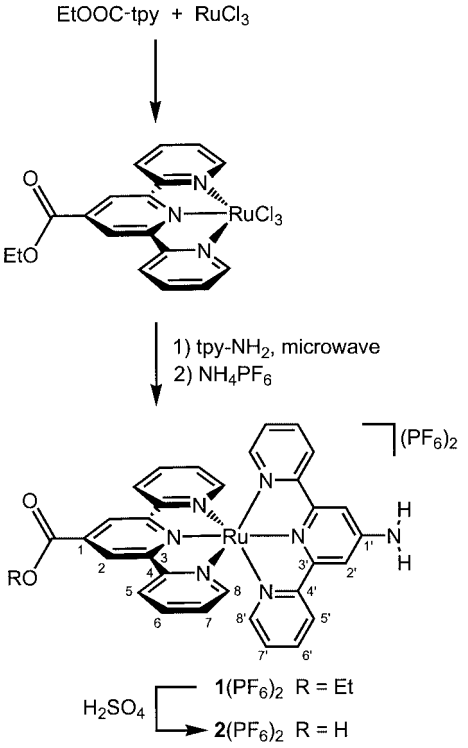


Scheme 1.

amine protons resonate at $\delta$ = 6.00 and the aliphatic protons of the ethyl group at $\delta$ = 4.64 and $\delta$ = 1.57 with expected intensity ratios (for full assignment see Table 1). The assignment of $^{13}$C NMR signals is summarised in the Exp. Sect. (Table 5). The FAB mass spectra establish the composition of $\mathbf{1}^{2+}$ showing signals for $[\mathbf{1} + H,PF_6]^+$ and $[\mathbf{1}]^+$ at $m/z$ = 801 and $m/z$ = 655, respectively. In the IR spectrum of $\mathbf{1}(PF_6)_2$ characteristic absorption bands are observed for the substituents and the hexafluorophosphate counterions (Table 2; Supporting Information, see footnote on the first page of this article).

Table 2. Characteristic IR spectroscopic data [$\tilde{\nu}$/cm$^{-1}$] of complexes $\mathbf{1}(PF_6)_2$–$\mathbf{5}(PF_6)_2$.

| | $\mathbf{1}(PF_6)_2$ | $\mathbf{2}(PF_6)_2$ | $\mathbf{3}(PF_6)_2$ | $\mathbf{4}(PF_6)_2$ | $\mathbf{5}(PF_6)_2$ |
|---|---|---|---|---|---|
| CO (ester/acid) | 1723 | 1719 | – | – | 1721 |
| Amide I | – | – | 1622 | 1668, 1619 | 1674 |
| Amide II | – | – | 1551 | 1574, 1560 | 1577 |
| $NH_2$ (def.) | 1636 | 1634 | 1634 | – | – |
| PF | 838 | 838 | 841 | 839 | 841 |

Hydrolysis of the ester moiety of $\mathbf{1}(PF_6)_2$ to the corresponding acid was unsuccessful with a catalytic amount of hydrochloric acid at room temperature and under microwave heating, while under more forcing conditions (20% sulfuric acid, reflux) the acid $\mathbf{2}(PF_6)_2$ was isolated in 74% yield (Scheme 1). The successful synthesis of $\mathbf{2}(PF_6)_2$ was confirmed by NMR and IR spectroscopy (Tables 1, 2 and 5) as well as mass spectrometry (see Exp. Sect.).

Single crystals have been obtained from an aqueous acidic solution of $\mathbf{2}(PF_6)_2$. The mixed salt $\mathbf{2}(PF_6)(F)$ crystallises in the triclinic space group $P\bar{1}$ with two independent cationic molecules in the asymmetric unit (Figure 1). The cations and anions are embedded in strands of solvent water (about 4–5 per ruthenium centre) held together by

Table 1. $^1$H NMR spectroscopic data of complexes $\mathbf{1}(PF_6)_2$–$\mathbf{5}(PF_6)_2$ in $CD_3CN$ (atom numbering according to Scheme 1).

| | $\mathbf{1}(PF_6)_2$ | $\mathbf{2}(PF_6)_2$[a] | $\mathbf{3}(PF_6)_2$ | $\mathbf{4}(PF_6)_2$ | $\mathbf{5}(PF_6)_2$ |
|---|---|---|---|---|---|
| $H^2$ | 9.15 (s, 2 H) | 9.18 (s, 2 H) | 9.16 (s, 2 H) | 9.16 (s, 2 H) | 9.20 (s, 2 H) |
| $H^5$ | 8.63 (d, 2 H, $^3J_{HH}$ = 8.0 Hz) | 8.63 (d, 2 H, $^3J_{HH}$ = 8.1 Hz) | 8.64 (d, 2 H, $^3J_{HH}$ = 7.5 Hz) | 8.65 (d, 2 H, $^3J_{HH}$ = 8.0 Hz) | 8.67 (d, 2 H, $^3J_{HH}$ = 8.0 Hz) |
| $H^6$ | 7.89 (m, 2 H) | 7.93 (m, 2 H) | 7.96 (m, 2 H) | 7.97 (m, 2 H) | 7.97 (m, 2 H) |
| $H^7$ | 7.26 (dd, 2 H, $^3J_{HH}$ = 5.4; $^4J_{HH}$ = 1.2 Hz) | 7.28 (dd, 2 H, $^3J_{HH}$ = 5.4; $^4J_{HH}$ = 1.2 Hz) | 7.26 (pt, 2 H) | 7.31 (pt, 2 H) | 7.26 (m, 2 H) |
| $H^8$ | 7.56 (d, 2 H, $^3J_{HH}$ = 5.0 Hz) | 7.55 (d, 2 H, $^3J_{HH}$ = 5.4 Hz) | 7.56 (d, 2 H, $^3J_{HH}$ = 5.4 Hz) | 7.52 (d, 2 H, $^3J_{HH}$ = 5.2 Hz) | 7.52 (d, 2 H, $^3J_{HH}$ = 5.0 Hz) |
| $H^{2'}$ | 7.96 (s, 2 H) | 7.98 (s, 2 H) | 7.97 (s, 2 H) | 9.24 (s, 2 H) | 9.28 (s, 2 H) |
| $H^{5'}$ | 8.26 (d, 2 H, $^3J_{HH}$ = 8.0 Hz) | 8.27 (d, 2 H, $^3J_{HH}$ = 8.1 Hz) | 8.27 (d, 2 H, $^3J_{HH}$ = 8.0 Hz) | 8.43 (d, 2 H, $^3J_{HH}$ = 8.0 Hz) | 8.45 (d, 2 H, $^3J_{HH}$ = 8.0 Hz) |
| $H^{6'}$ | 7.84 (m, 2 H) | 7.83 (m, 2 H) | 7.84 (m, 2 H) | 7.93 (m, 2 H) | 7.93 (m, 2 H) |
| $H^{7'}$ | 7.03 (dd, 2 H, $^3J_{HH}$ = 5.2; $^4J_{HH}$ = 1.2 Hz) | 7.03 (dd, 2 H, $^3J_{HH}$ = 5.2; $^4J_{HH}$ = 1.2 Hz) | 7.05 (pt, 2 H) | 7.14 (pt, 2 H) | 7.13 (pt, 2 H) |
| $H^{8'}$ | 7.16 (d, 2 H, $^3J_{HH}$ = 5.2 Hz) | 7.18 (d, 2 H, $^3J_{HH}$ = 5.2 Hz) | 7.22 (d, 2 H, $^3J_{HH}$ = 5.2 Hz) | 7.23 (d, 2 H, $^3J_{HH}$ = 5.4 Hz) | 7.28 (d, 2 H, $^3J_{HH}$ = 5.2 Hz) |
| $CH_2$ | 4.64 (q, 2 H, $^3J_{HH}$ = 7.1 Hz) | – | – | – | 4.67 (q, 2 H, $^3J_{HH}$ = 7.1 Hz) |
| $CH_3$ | 1.56 (t, 3 H, $^3J_{HH}$ = 7.1 Hz) | – | – | – | 1.59 (t, 3 H, $^3J_{HH}$ = 7.0 Hz) |
| $NH_2$ | 6.00 (br. s, 2 H) | 6.03 (br. s, 2 H) | 6.00 (br. s, 2 H) | – | – |
| NH | – | – | 9.21 (s, 1 H) | 9.08 (s, 1 H)[b] | – |
| NH′ | – | – | – | 9.31 (s, 1 H)[b] | 9.43 (s, 1 H) |
| Cp-H | | | 4.99 (s, 2 H), 4.29 (s, 5 H), 4.18 (s, 2 H) | 4.98 (s, 2 H), 4.31 (s, 5 H), 4.19 (s, 2 H) | |
| Cp′-H | – | – | | 5.14 (s, 2 H), 4.66 (s, 2 H), 4.41 (s, 5 H) | 5.17 (s, 2 H), 4.68 (s, 2 H), 4.42 (s, 5 H) |

[a] At pH 2. [b] Assignment according to NOE crosspeak NH′–Cp–H.

  

hydrogen bonds and involving both the acid and amine groups of the cations. Selected bond lengths and angles of the independent complex molecules (Table 3) show that both cations exhibit similar primary coordination geometries. However, the two cations display different secondary coordination spheres. The amine group of one cation is hydrogen-bonded to a hexafluorophosphate counterion while the amine group of the other cation is hydrogen-bonded to solvent water (Figure 1).

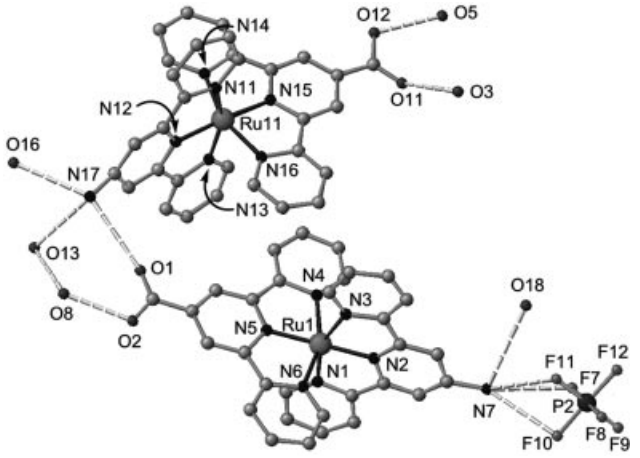


Figure 1. Two independent complex cations of $\mathbf{2}(PF_6)(F)$ and their partial secondary coordination sphere (O3, O5, O8, O13, O16 and O18 denote solvent water).

The acid group of $\mathbf{2}(PF_6)_2$ is activated by 1-hydroxybenzotriazole (HOBt) in the presence of 1,3-dicyclohexylcarbodiimide (DCC). Subsequent reaction with aminoferrocene[22] gives the C-terminal-substituted ferrocene conjugate $\mathbf{3}(PF_6)_2$ (Scheme 2). Under these conditions the less reactive aromatic amino group of $\mathbf{2}(PF_6)_2$ remains intact, thus the use of protective groups can be avoided.

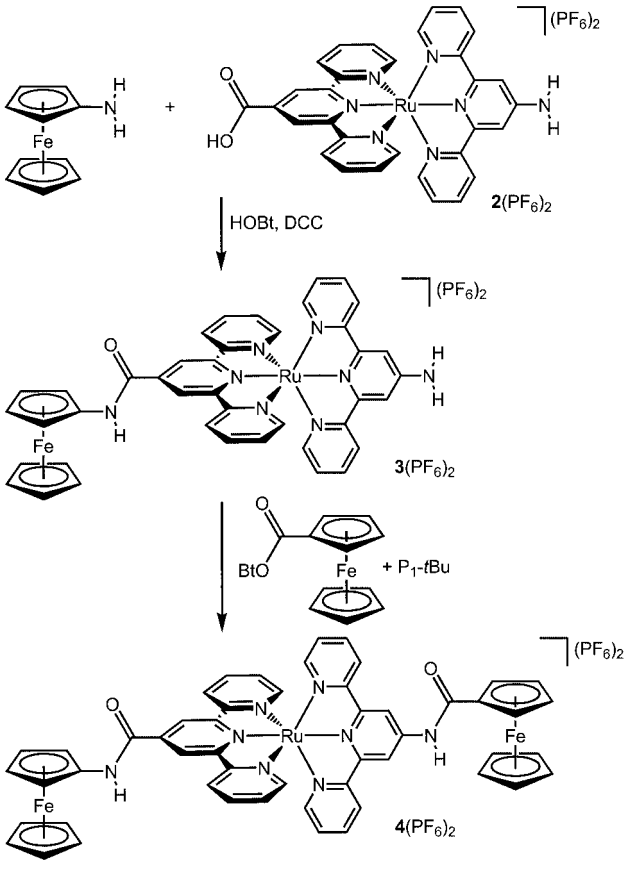


Scheme 2.

Under more forcing conditions employing the organic-soluble, nonionic Schwesinger phosphazene base $P_1$-*t*Bu[36–38] the amino groups of $\mathbf{1}(PF_6)_2$ and $\mathbf{3}(PF_6)_2$ form peptide bonds with ferrocenoyl benzotriazol ester Fc-CO-OBt[39] to give the N-terminal-substituted ferrocene conjugate $\mathbf{5}(PF_6)_2$ and the bis-ferrocene bisamide $\mathbf{4}(PF_6)_2$, respec-

Table 3. Experimental and DFT calculated selected bond lengths [Å] and angles [°] of $\mathbf{2}(PF_6)(F)$.

| | Ru1 | Ru11 | DFT | | Ru1 | Ru11 | DFT |
|---|---|---|---|---|---|---|---|
| Ru1–N1 | 2.082(9) | 2.063(9) | 2.111 | N1–Ru1–N2 | 78.3(4) | 79.2(4) | 78.4 |
| Ru1–N2 | 1.988(10) | 1.975(11) | 2.023 | N1–Ru1–N3 | 156.4(4) | 156.9(4) | 156.7 |
| Ru1–N3 | 2.077(8) | 2.101(8) | 2.111 | N1–Ru1–N4 | 94.7(4) | 89.7(4) | 92.1 |
| Ru1–N4 | 2.090(10) | 2.066(10) | 2.110 | N1–Ru1–N5 | 101.5(4) | 103.5(4) | 101.7 |
| Ru1–N5 | 1.969(9) | 1.974(10) | 1.998 | N1–Ru1–N6 | 89.3(4) | 94.7(4) | 92.1 |
| Ru1–N6 | 2.049(9) | 2.084(10) | 2.110 | N2–Ru1–N3 | 78.2(3) | 77.8(4) | 78.4 |
| C31–O1 | 1.211(16) | 1.231(16) | 1.230 | N2–Ru1–N4 | 101.7(4) | 104.2(4) | 100.9 |
| C31–O2 | 1.284(18) | 1.295(15) | 1.375 | N2–Ru1–N5 | 179.1(4) | 176.9(4) | 179.4 |
| N7···F7 | 3.0 | | – | N2–Ru1–N6 | 99.8(4) | 99.1(4) | 101.0 |
| N7···F10 | 3.3 | | – | N3–Ru1–N4 | 91.5(4) | 94.3(4) | 92.1 |
| N7···F11 | 3.2 | | – | N3–Ru1–N5 | 102.0(3) | 99.6(3) | 101.2 |
| N7···O18 | 3.5 | | – | N3–Ru1–N6 | 93.2(4) | 90.6(4) | 92.2 |
| N17···O1 | | 3.4 | – | N4–Ru1–N5 | 79.2(4) | 77.6(4) | 79.1 |
| N17···O13 | | 3.2 | – | N4–Ru1–N6 | 158.5(4) | 156.7(4) | 158.1 |
| N17···O16 | | 3.1 | – | N5–Ru1–N6 | 79.4(4) | 79.1(4) | 79.0 |
| O2···O8 | 2.6 | | – | O1–C31–O2 | 123(1) | 122(1) | 124.3 |
| O8···O13 | 2.8 | | – | | | | |
| O11···O3 | | 2.8 | – | | | | |
| O12···O5 | | 2.6 | – | | | | |

  

tively (Scheme 2 and Scheme 3). All ferrocene conjugates, **3**$(PF_6)_2$, **4**$(PF_6)_2$ and **5**$(PF_6)_2$, were fully characterised by NMR and IR spectroscopy (see Tables 1, 2, 5 and Supporting Information) as well as mass spectrometry and elemental analyses (see Exp. Sect.).

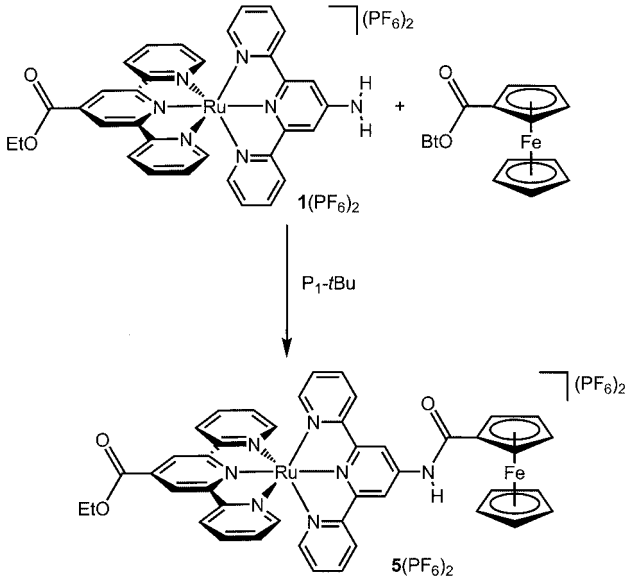


Scheme 3.

The amide protons of **3**$(PF_6)_2$, **4**$(PF_6)_2$ and **5**$(PF_6)_2$ resonate at low field around $\delta$ = 9.0–9.4 ppm. The signals of the cyclopentadienyl protons are found between $\delta$ = 4.2 and 5.2 ppm with typical chemical shifts of N- and C-substituted ferrocenes.[22,24,39] Amide formation at the N terminus of the terpyridine complex results in a downfield shift of the terpyridine proton signal $H^{2'}$ by 1.3 ppm, confirming the activation of the amino group.

## Acid/Base Equilibria of 2$(PF_6)_2$

Solubility and reactivity of **2**$(PF_6)_2$ strongly depends on the pH of the solution. Thus **2**$(PF_6)_2$ was investigated in aqueous solution at different pH values. The corresponding UV/Vis spectra are shown in Figure 2 and Figure 3. As can be deduced from the spectra, three different species exist in aqueous solution, which are assigned different protonated forms of $\mathbf{2}^{2+}$ namely $[\mathbf{2} - H]^+$, $[\mathbf{2}]^{2+}$ and $[\mathbf{2} + H]^{3+}$ (Scheme 4) with absorption maxima of the MLCT transitions at 494, 498 and 486 nm, respectively. Isosbestic points are observed in the spectra of $[\mathbf{2} - H]^+$ and $[\mathbf{2}]^{2+}$ at 494 and 531 nm (Figure 2) and in the spectra of $[\mathbf{2}]^{2+}$ and $[\mathbf{2} + H]^{3+}$ at 491 and 533 nm (Figure 3). The monocationic deprotonated carboxylate complex $[\mathbf{2} - H]^+$ exists at pH > 4 (up to pH ≈ 12 in aqueous solution) and the ammonium trication $[\mathbf{2} + H]^{3+}$ at pH < 0 (concentrated sulfuric acid), while the dication $[\mathbf{2}]^{2+}$ dominates in the intermediate pH range. The p$K_a$ values for the two protonation steps are p$K_{a1}$ = 2.69(8) and p$K_{a2}$ < 0, showing that $[\mathbf{2}]^{2+}$ is a stronger acid than benzoic acid and a weaker base than aniline.

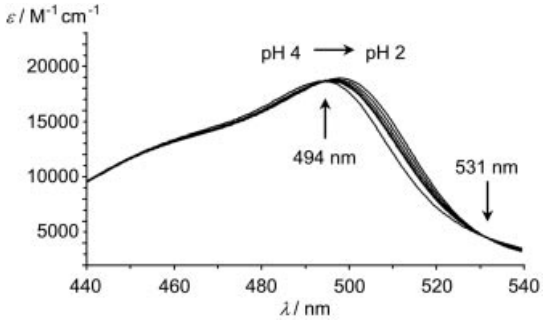


Figure 2. Absorption spectra of **2**$(PF_6)_2$ measured between pH 4 and pH 2.

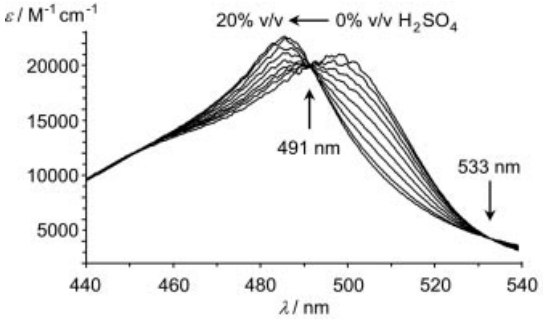


Figure 3. Absorption spectra of **2**$(PF_6)_2$ during titration with conc. sulfuric acid.

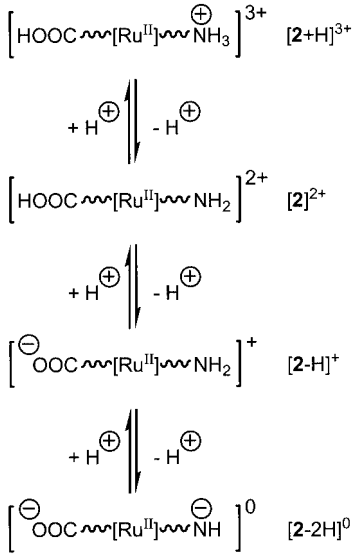


Scheme 4.

The strong base $P_1$-*t*Bu activates the amino groups in the ruthenium complexes **1**$(PF_6)_2$ and **3**$(PF_6)_2$ (see above). This can also be monitored in the UV/Vis spectra of **2**$(PF_6)_2$ during titration with $P_1$-*t*Bu in $CH_3CN$ (Figure 4). The acid group of $[\mathbf{2}]^{2+}$ is deprotonated first to give $[\mathbf{2} - H]^+$ (Figure 4 top, $\lambda_{max}$ = 491 nm; isosbestic points at 351, 474, 489 and 523 nm) and upon further addition of $P_1$-*t*Bu the amino group is deprotonated to give the neutral complex $[\mathbf{2} - 2H]^0$ with an absorption maximum at $\lambda_{max}$ = 493 nm (Figure 4 bottom, isosbestic points at 342, 423 and 515 nm).

  

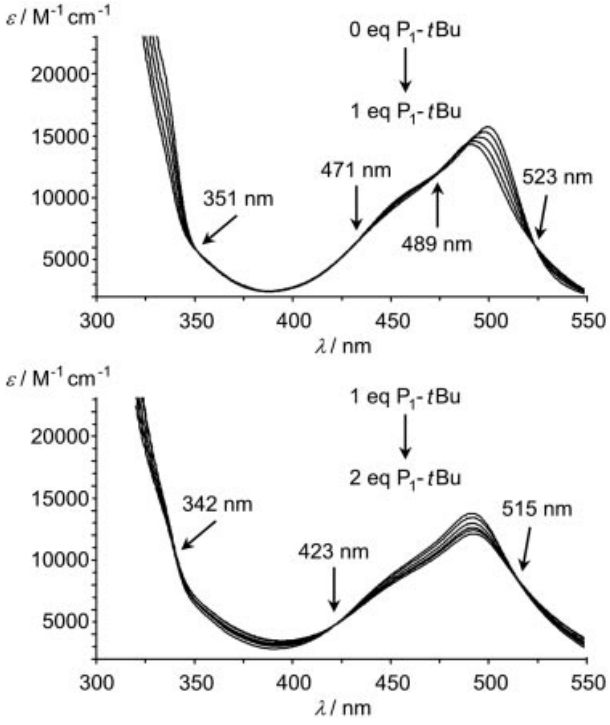


Figure 4. Absorption spectra of $\mathbf{2}(PF_6)_2$ during titration with $P_1$-*t*Bu in $CH_3CN$ from $[\mathbf{2}]^{2+}$ to $[\mathbf{2} - H]^+$ (top) and from $[\mathbf{2} - H]^+$ to $[\mathbf{2} - 2H]^0$ (bottom).

For both $[\mathbf{2} + H]^{3+}$ and $[\mathbf{2} - H]^+$ the low-energy $^1$MLCT absorption (involving the tpy-COOH and the tpy-$COO^-$ ligands, respectively; see below) is shifted to higher energy as compared to $[\mathbf{2}]^{2+}$. Protonation of the amino group renders the tpy-$NH_3^+$ ligand a weaker σ donor, thus decreasing the electron density at the metal centre and lowering the occupied metal-based orbitals.[12,40] Deprotonation of the COOH group of $[\mathbf{2}]^{2+}$ shifts the unoccupied orbitals of the tpy-$COO^-$ ligand to higher energies. Further deprotonation (of the $NH_2$ group) renders the tpy-$NH^-$ ligand a better donor, increasing the energy of the occupied ruthenium orbitals and thus shifting the $^1$MLCT absorption to lower energy. These simple molecular orbital arguments explain the experimentally observed relative positions of the absorption maxima of $[\mathbf{2} + H]^{3+}$, $[\mathbf{2}]^{2+}$, $[\mathbf{2} - H]^+$ and $[\mathbf{2} - 2H]^0$.

The proton NMR spectrum of $[\mathbf{2}]^{2+}$ (precipitated from solutions of pH 2) shows a singlet at $\delta = 6.03$ for the amine substituent with an intensity corresponding to two protons (Figure 5). At lower pH the amino group of $[\mathbf{2}]^{2+}$ is protonated to give $[\mathbf{2} + H]^{3+}$, which does not display any signal for the nitrogen-bonded hydrogen nuclei because of fast proton exchange. Raising the pH to 7 (presence of $[\mathbf{2} - H]^+$) results in downfield shifts of the $^1$H NMR signals of the amino group and the protons $H^2$ and $H^{2'}$ (Figure 5). Thus the NMR spectra confirm that the amine group is protonated only at pH < 2. On the other hand the IR spectrum of $[\mathbf{2}]^{2+}$ in dilute solution shows a signal at 1732 $cm^{-1}$, characteristic for a COOH group (see Supporting Information).

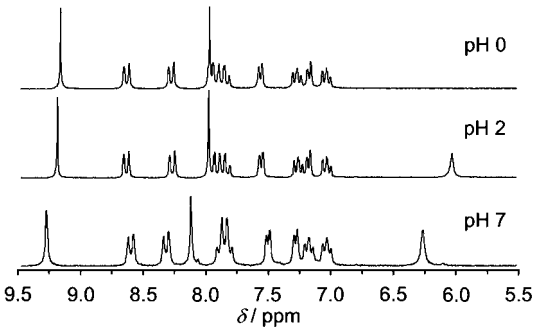


Figure 5. NMR spectra of $\mathbf{2}(PF_6)_2$ at pH 0, 2 and 7.

Thus the NMR and IR spectra provide evidence that $[\mathbf{2}]^{2+}$ does not form a zwitterion in solution in contrast to aliphatic amino acids with basic amino groups. This finding is easily explained by the very low basicity of the aromatic amino group of $[\mathbf{2}]^{2+}$.

### Electrochemistry, Absorption and Emission Spectra

Optical and electrochemical data of $\mathbf{1}(PF_6)_2$–$\mathbf{5}(PF_6)_2$ are collected in Table 4. For all complexes a ruthenium-centred oxidation is observed around 1.1 V versus SCE and two ligand-centred reductions are found around –1.2 V and –1.5 V (irr.). The ferrocene conjugates $\mathbf{3}(PF_6)_2$ and $\mathbf{5}(PF_6)_2$ undergo additional oxidations at 0.37 and 0.64 V, respectively, while $\mathbf{4}(PF_6)_2$ shows two further oxidation waves at 0.37 and 0.66 V corresponding to the two differently substituted ferrocene moieties in the oligonuclear species (Figure 6).

All compounds display two intense $^1$MLCT bands centred around 460–500 nm with a tail on the low-energy side extending as far as 650 nm and corresponding to spin-forbidden $^3$MLCT transitions around 550–600 nm, which become partially allowed because of spin-orbit coupling (Table 4, Figure 7). The $^1$MLCT bands undergo a slight bathochromic shift with increasing solvent polarity from acetonitrile to DMSO (Table 4).

For $\mathbf{3}(PF_6)_2$–$\mathbf{5}(PF_6)_2$, distinct transitions that could be assigned to ferrocene → terpyridine transitions have not been observed on the low-energy side of the absorption bands as found in, for example, $[Ru(tpy\text{-}Fc)_2](PF_6)_2$[42] or [(Fc-tpy)Ru(tpy-FcFc-tpy)Ru(tpy-Fc)]$(PF_6)_4$.[43] However, the extinction coefficients of the MLCT bands of $\mathbf{4}(PF_6)_2$ and $\mathbf{5}(PF_6)_2$ are significantly higher than those of $\mathbf{1}(PF_6)_2$–$\mathbf{3}(PF_6)_2$. The difference spectra "$\mathbf{4}(PF_6)_2 - \mathbf{3}(PF_6)_2$" and "$\mathbf{5}(PF_6)_2 - \mathbf{1}(PF_6)_2$" (Supporting Information) reveal an additional band around $\lambda_{max} \approx 493$ nm with $\varepsilon \approx 7000$ $M^{-1}cm^{-1}$, which could be assigned to a d(Fe) → π*(tpy-NHR′) transition originating from the C-substituted (the N-terminal) ferrocene to the electron-deficient aromatic tpy system.[22,42,43] Thus the $^1$MLCT region contains contributions arising from electron injection from the ruthenium centre and from the ferrocene [in the case of $\mathbf{4}(PF_6)_2$ and $\mathbf{5}(PF_6)_2$] into the differently substituted terpyridine ligands (see below).

  

Table 4. Cyclic voltammetric (vs. SCE), absorption and emission data of complexes $\mathbf{1}(PF_6)_2$–$\mathbf{5}(PF_6)_2$.

| | $\mathbf{1}(PF_6)_2$ | $\mathbf{2}(PF_6)_2$[a] | $\mathbf{3}(PF_6)_2$ | $\mathbf{4}(PF_6)_2$ | $\mathbf{5}(PF_6)_2$ |
|---|---|---|---|---|---|
| **CV**[b] | | | | | |
| $E_{1/2}$ [V] ($\Delta E$ [V]) $Ru^{II}/Ru^{III}$ | 1.08 (0.09) | 1.06 (0.08) | 1.30 (qrev.)[c] | 1.30 (0.19)[c] | 1.05 (0.15)[c] |
| $E_{1/2}$ [V] ($\Delta E$ [V]) $Fc/Fc^+$ | – | – | 0.37 (0.06) | 0.37 (0.11) | – |
| $E_{1/2}$ [V] ($\Delta E$ [V]) $Fc'/Fc'^+$ | – | – | – | 0.66 (0.12) | 0.64 (0.07) |
| $E_{1/2}$ [V] ($\Delta E$ [V]) $tpy/tpy^-$ | –1.14 (0.08), –1.59 (0.12) | –1.20 (irr.), –1.39 (irr.) | –1.21 (0.10), –1.6 (irr.) | –1.18 (0.12), –1.50 (irr.) | –1.10 (0.09), –1.55 (irr.) |
| **Absorption**[41] | | | | | |
| $\lambda_{max}$ [nm] ($\varepsilon$ [$M^{-1}cm^{-1}$])[b][f] | 557 (3690), 502 (19080), 467 (13790) | 570 (1900), 501 (20740), 467 (14370) | 601 (1830), 502 (19260), 479 (15630) | 597 (2380), 496 (25310), 477 (20030) | 583 (2350), 496 (26190), 476 (18270) |
| $\lambda_{max}$ [nm] ($\varepsilon$ [$M^{-1}cm^{-1}$])[d][f] | 560 (3700), 503 (19250), 472 (13550) | 569 (1700), 502 (20970), 469 (14600) | 612 (1610), 502 (18320), 478 (14910) | 601 (2290), 496 (25200), 478 (20090) | 546 (6570), 498 (25730), 478 (19080) |
| $\lambda_{max}$ [nm] ($\varepsilon$ [$M^{-1}cm^{-1}$])[e][f] | 562 (4170), 509 (19640), 475 (13810) | 571 (2230), 507 (20550), 474 (14390) | 626 (1260), 508 (19570), 482 (15820) | 547 (10950), 505 (26440), 485 (21470) | 552 (8940), 506 (26940), 477 (18240) |
| **Emission**[d] | | | | | |
| $\lambda_{max}$ [nm][g] | 799 | 739 | 739 | 704 | 704 |
| $\Phi$[h] | $3.4\times10^{-4}$ | $1.1\times10^{-4}$ | $<0.1\times10^{-4}$ | $<0.1\times10^{-4}$ | $1.1\times10^{-4}$ |
| $E_{0'-0}$ [eV][i] | 1.88 | 1.82 | n.d. | n.d. | 1.89 |

[a] Species obtained by precipitating from solutions of pH 2. [b] In acetonitrile. [c] These waves are no more reversible as oxidation to a highly charged species (+4, +5) results in precipitation of the complexes on the electrode. [d] In acetone. [e] In DMSO. [f] The extinction coefficients $\varepsilon$ are the experimentally observed values at the fitted band maxima. [g] Excitation at low-energy $^1$MLCT absorption maximum. [h] Luminescence quantum yield (±15%), using fluorescein in ethanol as standard. [i] Determined by fitting the emission data to Meyers equation.[44]

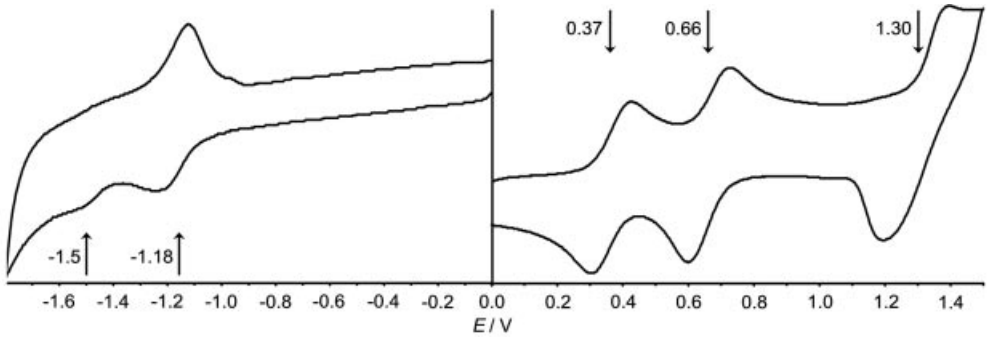


Figure 6. Cyclic voltammogram of $\mathbf{4}(PF_6)_2$ in $CH_3CN/nBu_4NPF_6$.

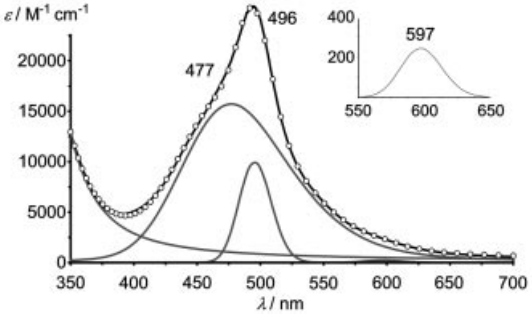


Figure 7. Absorption spectrum of $\mathbf{4}(PF_6)_2$ in $CH_3CN$ and calculated band profiles (the open circles represent the sum of the calculated profiles[41]). The inset shows an expansion of the $^3$MLCT region (fitted band profile).

All complexes are luminescent in argon-saturated acetone at room temperature ($\lambda_{max} \approx$ 700–800 nm; Table 4), although intensity is very weak for $\mathbf{3}(PF_6)_2$ and $\mathbf{4}(PF_6)_2$ ($\Phi < 0.1\times10^{-4}$). Deactivation of the emitting state ($^3$MLCT) in the parent complex $[Ru(tpy)_2]^{2+}$ occurs through a $^3$MC(Ru) state.[1,12] In complexes $\mathbf{1}(PF_6)_2$–$\mathbf{5}(PF_6)_2$ the $^3$MC(Ru) state is shifted to higher energy because of the stronger averaged ligand field raising the energy of the $e_g$ (Ru) orbitals and increasing the $^3$MLCT–$^3$MC(Ru) energy gap.[1,12]

The emission spectra of $\mathbf{1}(PF_6)_2$, $\mathbf{2}(PF_6)_2$ and $\mathbf{5}(PF_6)_2$ could be fitted to the Meyers equation[44] with $E_{0'-0}$ around 1.9 eV (Figure 8). The emission properties of $\mathbf{2}(PF_6)_2$ strongly depend on the pH with higher luminescence quantum yield ($\Phi = 2.1\times10^{-4}$ in water) between pH > 4 and pH < 10 (corresponding to the presence of $[\mathbf{2} - H]^+$, see above) and weak emission at either lower or higher pH ($\Phi = 0.6\times10^{-4}$ in water; see Supporting Information).

For $\mathbf{1}(PF_6)_2$ and $\mathbf{2}(PF_6)_2$ emission gains intensity with increasing excitation wavelength ($\lambda_{exc}$ = 500–650 nm), while for $\mathbf{5}(PF_6)_2$ the reverse is observed (see Supporting Infor-

  

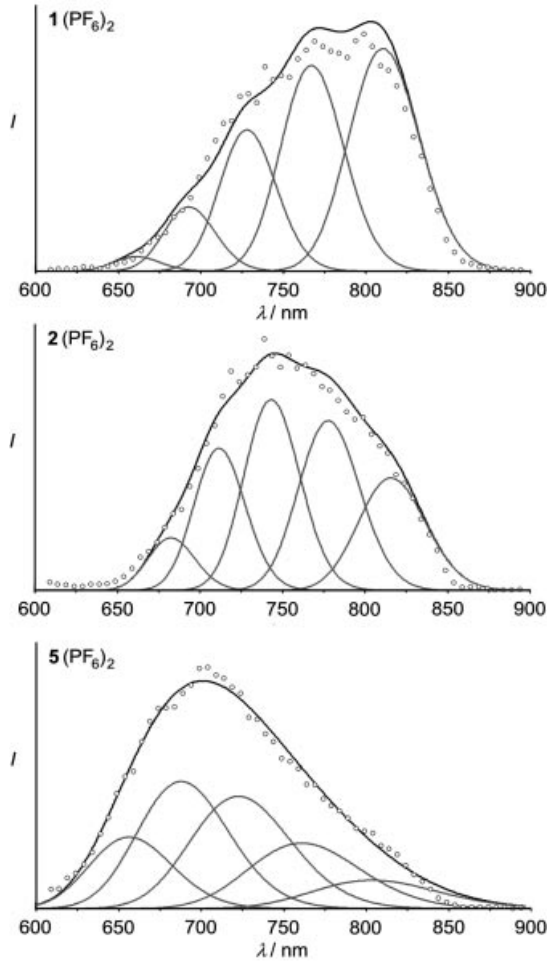


Figure 8. Emission spectra of **1**$(PF_6)_2$, **2**$(PF_6)_2$ and **5**$(PF_6)_2$ (○) in acetone at room temperature and spectral fitting according to Meyers equation.[44]

mation). The C-terminal ferrocene conjugates **3**$(PF_6)_2$ and **4**$(PF_6)_2$ show a much weaker luminescence than their ester analogues **1**$(PF_6)_2$ and **5**$(PF_6)_2$, respectively (Table 4).[45]

### DFT Calculations

All complex cations $\mathbf{1}^{2+}$–$\mathbf{5}^{2+}$ were studied using the B3LYP/LanL2DZ functional. The energy-minimised structure of $\mathbf{5}^{2+}$ shown in Figure 9 as an example shows the expected pseudo-octahedral geometry around the ruthenium centre. The geometric results of the calculation for $\mathbf{2}^{2+}$ reproduce the experimental data of **2**$(PF_6)$(F) sufficiently well (Table 3).

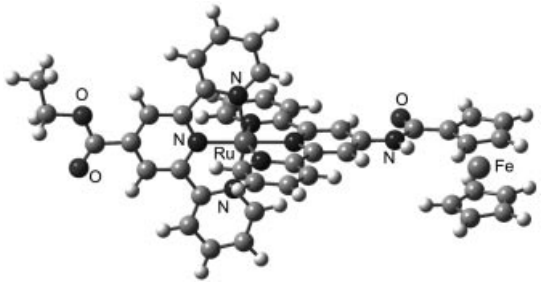


Figure 9. Energy-minimised structure of $\mathbf{5}^{2+}$.

The frontier orbital region of the complex cations consists of closely spaced molecular orbitals (Figure 10). The lowest unoccupied molecular orbitals are π* orbitals of the terpyridine ligands with the LUMO level lying 0.2–0.3 eV below the next highest virtual orbital. Throughout the series the LUMO is localised on the C-terminal terpyridine (tpy-COR). The "$t_{2g}$" manifold of the ruthenium centre provides the high-lying occupied orbitals. For the ferrocene conjugates $\mathbf{3}^{2+}$–$\mathbf{5}^{2+}$ molecular orbitals composed of iron and cyclopentadienyl moieties are inserted in between (Figure 10). The C-terminal ferrocene orbitals d(Fe) + π*(Cp-NHR′′) are found at higher energies than the N-terminal ferrocene orbitals d(Fe) + π*(Cp-COR′′′), as expected from the respective oxidation potentials (Table 4).

The $^1$MLCT transitions arise from $t_{2g}$ (Ru) → π*(tpy) excitations. The low-energy transition (≈500 nm) can be assigned to involve the C-terminal terpyridine tpy-COR, while the next highest transitions (≈480 nm) can be assigned to involve mixtures of both terpyridine ligands tpy-NHR′ and tpy-COR. Low-energy d(Fe) → π*(tpy-NHR′) transitions were observed experimentally for **4**$(PF_6)_2$ and **5**$(PF_6)_2$ around 493 nm with significant intensity (Supporting Information).

A schematic energy level diagram (Figure 11) shows the typical ruthenium $^1$MLCT and $^3$MLCT states. The numerical values are estimates using experimental data obtained under different conditions, thus some caution in their interpretation is advisable. The UV/Vis spectroscopic data

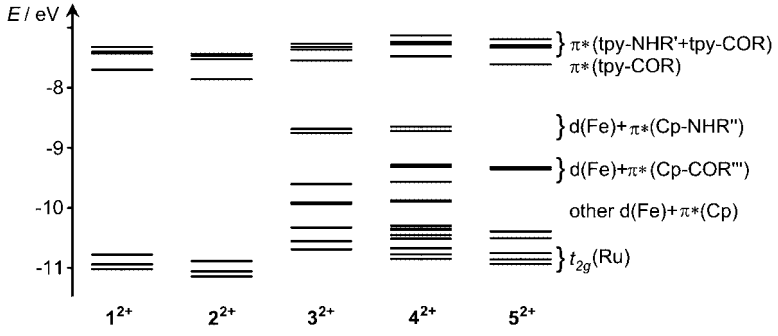


Figure 10. Partial molecular orbital diagrams for $\mathbf{1}^{2+}$–$\mathbf{5}^{2+}$.

  

provide estimates for the energies of the Franck–Condon excited $^1$MLCT states around 2.5 eV. The emission data indicate that the energy level of the emitting $^3$MLCT state has an energy around 1.9 eV,[44] which fits to the Franck-Condon excited $^3$MLCT state (not shown in Figure 11), estimated to be around 2.1–2.2 eV (Table 4).

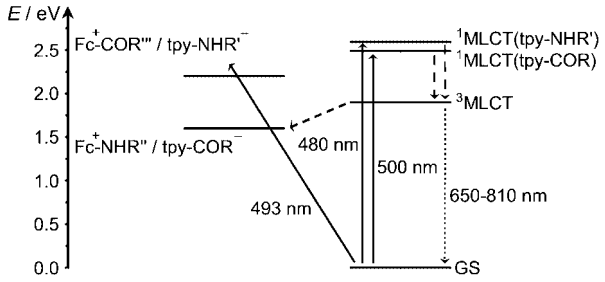


Figure 11. Schematic Jablonski-type energy level diagram (solid lines: excitation; dashed lines: intersystem crossing and electron transfer; dotted line: emission).

Excitation of **1**$(PF_6)_2$ or **2**$(PF_6)_2$ with $\lambda_{exc}$ = 480–500 nm will populate the $^1$MLCT states that undergo intersystem crossing to the emitting $^3$MLCT state while excitation of **1**$(PF_6)_2$ or **2**$(PF_6)_2$ with $\lambda_{exc} > 500$ nm will also directly populate the $^3$MLCT state leading to the experimentally observed increase of the emission intensity (see above; Supporting Information).

For **3**$(PF_6)_2$–**5**$(PF_6)_2$ states arising from the presence of the ferrocene moieties are depicted on the left side of Figure 11. The Franck–Condon excited state d(Fe) → π*(tpy-NHR′) could be observed for **4**$(PF_6)_2$ and **5**$(PF_6)_2$ in the UV/Vis difference spectra around 493 nm (see above and Supporting Information). The ferrocene oxidation potentials and ligand reduction potentials of **3**$(PF_6)_2$–**5**$(PF_6)_2$ (Table 4) allow approximation of the energies of the charge separated states [$Fc^+$-COR′′′/tpy-NHR′$^-$] and [$Fc^+$-NHR′′/tpy-$COR^-$] by 2.2 and 1.6 eV. The former level lies above and the latter below the emitting $^3$MLCT state of the ruthenium core. For **3**$(PF_6)_2$ and **4**$(PF_6)_2$ with a C-terminal ferrocene photoinduced electron transfer is exergonic by 0.3 eV while for **5**$(PF_6)_2$ containing an N-terminal ferrocene photoinduced electron transfer would be endergonic by 0.3 eV. Thus reductive electron transfer from ferrocene to ruthenium is conceivable for **3**$(PF_6)_2$ and **4**$(PF_6)_2$ but not for **5**$(PF_6)_2$, accounting for the experimentally observed luminescence quenching (Table 4).

In contrast to **1**$(PF_6)_2$ and **2**$(PF_6)_2$, direct population of the $^3$MLCT state of **5**$(PF_6)_2$ is hampered because of the population of the d(Fe) → π*(tpy-NHR′) state leading to the experimentally observed decrease in emission intensity at $\lambda_{exc} > 500$ nm (see above and Supporting Information).

The low-lying ferrocene triplet state (not shown in the diagram) has been estimated at an energy between 1.1 and 1.8 eV,[1] that is, in the same energy range as the $^3$MLCT and charge-separated states. Thus energy transfer might also be an additional channel for radiationless excited-state decay.[46–50] Further photophysical investigations including low-temperature emission spectroscopy, lifetime measurements and transient absorption spectroscopy as well as DFT calculations on excited states are currently underway.

## Conclusion

The amino-substituted acid **2**$(PF_6)_2$ and its ester **1**$(PF_6)_2$ have been synthesised and characterised. Complex $\mathbf{2}^{2+}$ undergoes several protonation and deprotonation steps, which have been observed by UV/Vis and emission spectroscopy as well as NMR spectroscopy. Amide formation of **1**$(PF_6)_2$ or **2**$(PF_6)_2$ with ferrocene derivatives was successful in spite of the low reactivity of the aromatic amino group. Ferrocenes have been attached on either side or on both sides of the bis(terpyridine) ruthenium(II) core [**3**$(PF_6)_2$–**5**$(PF_6)_2$].

The ground-state electronic situation of these multinuclear species has been investigated by electronic spectroscopy and cyclic voltammetry, while preliminary emission studies gave insight into the excited-state properties. The ground-state properties of the bis(terpyridine) ruthenium(II) moiety are only slightly modified by the presence of the ferrocenes. The exception is an additional charge-transfer band observed in the absorption spectra of **4**$(PF_6)_2$ and **5**$(PF_6)_2$ but not in the spectra of **3**$(PF_6)_2$. This transition is associated with N-terminal bound ferrocenes and has been assigned d(Fe) → π*(tpy-NHR′) charge transfer character.

The excited-state behaviour of the ferrocene conjugates is strongly dependent on the site of ferrocene attachment: **5**$(PF_6)_2$ with an N-terminal bound ferrocene is luminescent with an inverse correlation to the excitation wavelength as compared to the ferrocene-free **1**$(PF_6)_2$. This behaviour arises from the presence of d(Fe) → π*(tpy-NHR′) charge-transfer bands. Complexes **3**$(PF_6)_2$ and **4**$(PF_6)_2$ with C-terminal bound ferrocenes are much less luminescent. This finding is explained on the assumption that electron transfer from the ferrocene to the ruthenium centre efficiently quenches the $^3$MLCT state of ruthenium.

Thus the optical ground-state properties of the bis(ferrocene) conjugate **4**$(PF_6)_2$ resemble those of the N-terminal conjugate **5**$(PF_6)_2$, while its excited-state properties are analogous to those of the C-terminal conjugate **3**$(PF_6)_2$.

To expand the scope of this design strategy we currently build larger arrays from ruthenium and ferrocene amino acids as well as chiral α-amino acids[22–24] using peptide chemistry for application in electron storage devices, molecular wires, photosensitisers and molecular sensors.

## Experimental Section

**General Methods:** Unless otherwise noted, starting materials were obtained from commercial suppliers and used without further purification. The terpyridine ligands tpy-COOEt[33] and tpy-$NH_2$[34,35] as well as the ferrocene derivatives[22,39] were synthesised according to literature procedures.

NMR spectra were recorded with a Bruker Avance DPX 200 at 200.15 MHz ($^1$H) and 50.323 MHz ($^{13}$C); chemical shifts ($\delta$) in ppm with respect to residual solvent peaks as internal standards:

  

$CD_3CN$ ($^1H$: $\delta$ = 1.93; $^{13}C$: $\delta$ = 1.3 ppm). IR spectra were recorded with a BioRad Excalibur FTS 3000 spectrometer using $CaF_2$ cells or CsI disks. UV/Vis/NIR spectra were recorded with a Perkin–Elmer Lambda 19, 0.2-cm cells (Hellma, suprasil). Cyclic voltammetry was performed using a glassy carbon electrode, a platinum electrode and a SCE electrode, $10^{-3}$ M in 0.1 M $n$Bu$_4$NPF$_6$/$CH_3CN$; potentials are given relative to that of SCE. Mass spectra were recorded with a Finnigan MAT 8400 spectrometer. Emission spectra were recorded with a Varian Cary Eclipse Fluorescence Spectrometer, slit widths 5 nm, in argon-saturated solution. Quantum yields were determined by comparing the areas under the emission spectra recorded for optically matched solutions of the samples and the fluorescein reference ($\Phi$ = 0.79 in ethanol). Elemental analyses were performed by the microanalytical laboratory of the Organic Chemistry Department, University of Heidelberg. Microwave-assisted reactions were performed in a domestic microwave oven operating at a frequency of 2450 MHz and maximum power of 700 W in 20-mL test tubes (Rotilabo).

**Computational Method:** Density functional calculations were carried out with the Gaussian03/DFT[51] series of programs. The B3LYP formulation of density functional theory was used employing the LanL2DZ basis set.[51] All structures were characterised as minima by frequency analysis ($N_{imag}$ = 0) except **3**$^{2+}$, which shows one imaginary frequency for Cp rotation (–10.4 cm$^{-1}$).

**X-ray Crystallography:** Data were collected with an Enraf–Nonius Kappa CCD diffractometer using graphite-monochromated Mo-$K_\alpha$ radiation. The data were processed using the standard Nonius software.[52] All calculations were performed using the SHELXT PLUS software package. Structures were solved using direct or Patterson methods with the SHELXS-97 program and refined with the SHELXL-97 program.[53] Graphical handling of the structural data during refinement was performed using XMPA[54] and WinRay.[55] Atomic coordinates and anisotropic thermal parameters were refined by full-matrix least-squares calculations on $F^2$.

Crystal dimensions 0.1 × 0.02 × 0.02 mm; triclinic crystal system; space group $P\bar{1}$; $a$ = 8.6940(17), $b$ = 21.412(4), $c$ = 21.588(4) Å; $\alpha$ = 94.86(3); $\beta$ = 96.52(3); $\gamma$ = 101.01(3)°; $V$ = 3895.9(13) Å$^3$; $\rho_{calcd.}$ = 1.474 g cm$^{-3}$; $2\theta_{max}$ = 50.1°; $\omega$-scans; $T$ = 200 K; measured reflections 21949; independent reflections 13619; observed reflections 6146 [$I > 2\sigma(I)$]; Lorentz and polarisation correction; $\mu$ = 0.530 mm$^{-1}$; $R_1$ = 0.102 [$I > 2\sigma(I)$]; $wR_2$ = 0.271 [$I > 2\sigma(I)$]; residual electron density 0.915 e Å$^{-3}$.

Because of the large amount of solvent water present in the crystal of **2**(PF$_6$)(F) causing diffuse reflection data and the rather poor data/parameter ratio, carbon atoms, solvent water, some counterions and hydrogen atoms have been refined isotropically.

CCDC-280162 contains the supplementary crystallographic data for this paper. These data can be obtained free of charge from The Cambridge Crystallographic Data Centre via www.ccdc.cam.ac.uk/data_request/cif.

**Synthesis of 1(PF$_6$)$_2$:** (EtOOC-tpy)RuCl$_3$[33–35] (200 mg, 0.39 mmol) and tpy-NH$_2$ (97 mg, 0.39 mmol) were finely suspended in dry ethanol (15 mL) with the aid of an ultrasonic bath. The test tube was closed and heated in the microwave oven for 5 × 1 min at the lowest operating power (80 W). The solution was filtered through a small pad of Celite, washed with water, and $NH_4PF_6$ (191 mg, 1.17 mmol) dissolved in 1 mL water was added. After cooling for 12 h to 4 °C the red product was collected by filtration, washed with water and dried in vacuo. Yield 85% (312 mg, 0.33 mmol). MS (FAB): $m/z$ (%) = 801 (11) [M + H,PF$_6$]$^+$, 655 (55) [M$^+$]. $C_{33}H_{27}F_{12}N_7O_2P_2Ru$ (944.6): calcd. C 41.96, H 2.88, N 10.38; found C 42.09, H 3.15, N 10.22. $^{13}C$ NMR data see Table 5.

**Synthesis of 2(PF$_6$)$_2$:** **1**(PF$_6$)$_2$ (250 mg, 0.27 mmol) was dissolved in 20% sulfuric acid (50 mL) and heated under reflux for 2 h. After cooling to room temperature and adjusting the pH to 2 with $NaOH_{aq}$, $NH_4PF_6$ (132 mg, 0.81 mmol) dissolved in 1 mL water was added and the product precipitated. The red product was collected by filtration, washed with water and dried. Yield 74% (185 mg, 0.20 mmol). MS (FAB): $m/z$ (%) = 772 (60) [M, PF$_6$]$^+$, 626 (100) [M$^+$ – H]. $C_{31}H_{23}F_{12}N_7O_2P_2Ru$ (916.6): calcd. C 40.62, H 2.53, N 10.70; found C 40.63, H 3.20, N 10.65. $^{13}C$ NMR data see Table 5.

**Synthesis of 3(PF$_6$)$_2$:** **2**(PF$_6$)$_2$ (150 mg, 0.16 mmol) was activated with HOBt (34 mg, 0.25 mmol) and DCC (52 mg, 0.25 mmol) in acetonitrile (25 mL) for 2.5 h. A solution of aminoferrocene (51 mg, 0.25 mmol) and *N*-ethylmorpholine (0.1 mL) in acetonitrile (5 mL) was added and the reaction mixture was stirred at room temperature for 2.5 h. The solvent was removed in vacuo, the residue was dissolved in dichloromethane and the product was

Table 5. $^{13}C$ NMR spectroscopic data of complexes **1**(PF$_6$)$_2$–**5**(PF$_6$)$_2$ in $CD_3CN$ (atom numbering according to Scheme 1).

| | **1**(PF$_6$)$_2$ | **2**(PF$_6$)$_2$[a] | **3**(PF$_6$)$_2$ | **4**(PF$_6$)$_2$ | **5**(PF$_6$)$_2$ |
|---|---|---|---|---|---|
| C$^1$ | 135.6 | 135.3 | 159.5 | 156.6 | 136.6 |
| C$^2$ | 125.0 | 125.0 | 121.6 | 121.7 | 123.1 |
| C$^{3,3',4,4'}$ | 158.7, 158.4, 157.5, 156.5 | 158.7, 158.4, 157.5, 156.5 | 158.8, 158.6, 157.1, 156.4 | 158.6, 158.5, 158.3, 158.1 | 158.4, 158.2, 157.0, 155.2 |
| C$^5$ | 124.2 | 124.2 | 124.8 | 125.0 | 124.8 |
| C$^6$ | 138.2 | 138.2 | 138.2 | 138.5 | 138.5 |
| C$^7$ | 128.3 | 128.3 | 128.2 | 128.2 | 128.3 |
| C$^8$ | 152.5 | 152.5 | 152.6 | 152.9 | 152.7 |
| C$^{1'}$ | 154.4 | 154.4 | 154.5 | 155.3 | 148.0 |
| C$^{2'}$ | 109.1 | 109.1 | 109.1 | 114.0 | 114.0 |
| C$^{5'}$ | 122.9 | 123.3 | 124.2 | 124.7 | 125.2 |
| C$^{6'}$ | 138.6 | 138.6 | 138.5 | 138.8 | 138.8 |
| C$^{7'}$ | 127.4 | 127.4 | 127.4 | 127.9 | 127.8 |
| C$^{8'}$ | 153.2 | 153.1 | 153.1 | 153.1 | 153.2 |
| $CH_2$ | 63.2 | – | – | – | 63.3 |
| $CH_3$ | 14.1 | – | – | – | 14.1 |
| C=O | n.o.[b] | 165.1 | 162.6 | n.o.[b] | 164.5 |
| C′=O | – | – | – | n.o.[b] | 171.2 |
| Cp–C | – | – | 69.7 ($C_5H_5$), 65.4, 62.4[c] | 69.8 ($C_5H_5$), 65.4, 62.4[c] | – |
| Cp′–C | – | – | – | 70.6 ($C_5H_5$), 72.5, 69.5[c] | 70.6 ($C_5H_5$), 72.5, 69.5[c] |

[a] At pH 2. [b] n.o., not observed. [c] $C_{ipso}$ of the cyclopentadienyl rings not observed.

  

precipitated by adding diethyl ether. Recrystallisation from hot ethanol and precipitating with $NH_4PF_6$ (78 mg, 0.48 mmol) dissolved in 1 mL water gave the pure product. Yield 88% (150 mg, 0.14 mmol). MS (FAB): *m*/*z* (%) = 810 (40) [$M^+$ – H]. $C_{41}H_{32}F_{12}FeN_8OP_2Ru{\cdot}2H_2O$ (1099.6·$2H_2O$): calcd. C 43.36, H 3.20, N 9.87; found C 43.44, H 3.61, N 10.07. $^{13}C$ NMR data see Table 5.

**Synthesis of 4(PF$_6$)$_2$:** **3**$(PF_6)_2$ (100 mg, 0.09 mmol), ferrocenoyl benzotriazol ester Fc-COOBt (38 mg, 0.11 mmol) and phosphazene base $P_1$-*t*Bu (43 mg, 0.18 mmol) were dissolved in acetonitrile (15 mL) and stirred at room temperature for 16 h. The solvent was removed in vacuo, the residue was dissolved in dichloromethane and the product was precipitated by adding diethyl ether. Recrystallisation from hot ethanol and precipitating with $NH_4PF_6$ (44 mg, 0.27 mmol) dissolved in 1 mL water gave the pure product. Yield 89% (110 mg, 0.08 mmol). MS (FAB): *m*/*z* (%) = 1167 (92) [M, $PF_6$]$^+$, 1021 (100) [$M^+$ – H]. $C_{52}H_{40}F_{12}Fe_2N_8O_2P_2Ru{\cdot}5H_2O$ (1311.6·$5H_2O$): calcd. C 44.56, H 3.60, N 7.99; found C 44.40, H 3.60, N 8.11. $^{13}C$ NMR data see Table 5.

**Synthesis of 5(PF$_6$)$_2$:** **2**$(PF_6)_2$ (100 mg, 0.11 mmol), ferrocenoyl benzotriazol ester Fc-COOBt (37 mg, 0.11 mmol) and phosphazene base $P_1$-*t*Bu (53 mg, 0.22 mmol) were dissolved in acetonitrile (15 mL) and stirred at room temperature for 16 h. The solvent was removed in vacuo, the residue was dissolved in dichloromethane and the product was precipitated by adding diethyl ether. Recrystallisation from hot ethanol and precipitating with $NH_4PF_6$ (54 mg, 0.33 mmol) dissolved in 1 mL water gave the pure product. Yield 91% (115 mg, 0.10 mmol). MS (FAB): *m*/*z* (%) = 1113 (50) [M + H, $PF_6$]$^+$, 866 (100) [$M^+$ – H]. $C_{44}H_{35}F_{12}FeN_7O_3P_2Ru{\cdot}H_2O$ (1156.6·$H_2O$): calcd. C 44.99, H 3.17, N 8.35; found C 44.96, H 3.52, N 8.68. $^{13}C$ NMR data see Table 5.

**Supporting Information Available** (for details see the footnote on the first page of this article): Absorption spectra of **1**$(PF_6)_2$–**5**$(PF_6)_2$ in $CH_3CN$, difference spectrum "**3**$(PF_6)_2$ – **1**$(PF_6)_2$", difference spectrum "**4**$(PF_6)_2$ – **3**$(PF_6)_2$", difference spectrum "**5**$(PF_6)_2$ – **1**$(PF_6)_2$", IR spectra of **1**$(PF_6)_2$, **2**$(PF_6)_2$ and **5**$(PF_6)_2$ in $CH_3CN$, emission spectra of **3**$(PF_6)_2$ and **4**$(PF_6)_2$ with excitation at $\lambda_{max}$ in acetone at room temperature, emission spectra of **2**$(PF_6)_2$ at different pH in water (excitation wavelength 497 nm) at room temperature, pH profile of the emission of **2**$(PF_6)_2$ (excitation wavelength 497 nm, monitored at $\lambda$ = 719 nm), emission spectra of **1**$(PF_6)_2$, **2**$(PF_6)_2$ and **5**$(PF_6)_2$ with different excitation wavelengths in acetone at room temperature, excitation profiles of **1**$(PF_6)_2$, **2**$(PF_6)_2$ and **5**$(PF_6)_2$ in acetone at room temperature, Cartesian coordinates of DFT calculated geometries of **1**$^{2+}$–**5**$^{2+}$, molecular orbital energies (eV) of selected orbitals of **1**$^{2+}$–**5**$^{2+}$, absorption spectrum of **2**$(PF_6)_2$ in $CH_3CN$ in the range 250–800 nm.

## Acknowledgments

This work was supported by the Deutsche Forschungsgemeinschaft, the Fonds der Chemischen Industrie and the Dr. Otto Röhm Gedächtnisstiftung. The permanent, generous support from Prof. Dr. G. Huttner is gratefully acknowledged. We thank Simone Leingang and Jens Nägele for preparative assistance.

[1] J.-P. Sauvage, J.-P. Collin, J.-C. Chambron, S. Guillerez, C. Coudret, V. Balzani, F. Barigelletti, L. De Cola, L. Flamigni, *Chem. Rev.* **1994**, *94*, 993–1019.
[2] V. Balzani, A. Juri, M. Venturi, S. Campagna, S. Serroni, *Chem. Rev.* **1996**, *96*, 759–833.
[3] C. E. Housecroft in *Comprehensive Coordination Chemistry II* (Eds.: J. A. McCleverty, T. J. Meyer), Elsevier, Oxford, **2004**, vol. 5, pp. 555–731.
[4] A.-M. Stadler, F. Puntoriero, S. Campagna, N. Kyritsakas, F. Welter, J.-M. Lehn, *Chem. Eur. J.* **2005**, *11*, 3997–4009.
[5] J. Hjelm, R. W. Handel, A. Hagfeld, E. C. Constable, C. E. Housecroft, R. J. Foster, *Inorg. Chem.* **2005**, *44*, 1073–1081.
[6] R. Ziessel, P. Bäuerle, M. Ammann, A. Barbieri, F. Barigelletti, *Chem. Commun.* **2005**, 802–804.
[7] R. Ziessel, V. Grosshenny, M. Hissler, C. Stroh, *Inorg. Chem.* **2004**, *43*, 4262–4271.
[8] A. Barbieri, B. Ventura, F. Barigelletti, A. De Nicola, M. Quesada, R. Ziessel, *Inorg. Chem.* **2004**, *43*, 7359–7368.
[9] A. Harriman, A. Mayeux, C. Stroh, R. Ziessel, *Dalton Trans.* **2005**, 2925–2932.
[10] C. Patoux, J.-P. Launay, M. Beley, S. Chodorowski-Kimmes, J.-P. Collin, S. James, J.-P. Sauvage, *J. Am. Chem. Soc.* **1998**, *120*, 3717–3725.
[11] J. R. Soonover, D. M. Dattelbaum, A. Malko, V. I. Klimov, T. J. Meyer, D. J. Styers-Barnett, E. Z. Gannon, J. C. Granger, W. S. Aldridge, J. M. Papanikolas, *J. Phys. Chem. A* **2005**, *109*, 2472–2475.
[12] W. R. Browne, N. M. O'Boyle, J. J. McGarvey, J. G. Vos, *Chem. Soc. Rev.* **2005**, *34*, 641–663.
[13] Md. K. Nazeeruddin, M. Grätzel in *Comprehensive Coordination Chemistry II* (Eds.: J. A. McCleverty, T. J. Meyer), Elsevier, Oxford, **2004**, vol. 9, pp. 719–758.
[14] A. Hagfeldt, M. Grätzel, *Acc. Chem. Res.* **2000**, *33*, 269–277.
[15] T. J. Meyer, *Acc. Chem. Res.* **1989**, *22*, 163–170.
[16] E. Baranoff, J.-P. Collin, L. Flamigni, J.-P. Sauvage, *Chem. Soc. Rev.* **2004**, *33*, 147–155.
[17] M. Grätzel, *Inorg. Chem.* **2005**, *44*, 6841–6851.
[18] E. C. Constable in *Comprehensive Coordination Chemistry II* (Eds.: J. A. McCleverty, T. J. Meyer), Elsevier, Oxford, **2004**, vol. 7, pp. 263–302.
[19] M.-C. Daniel, J. Ruiz Aranzaes, D. Astruc, *Chem. Commun.* **2005**, 1569–1571.
[20] N. Sewald, H.-D. Jakubke, *Peptides: Chemistry and Biology*, Wiley-VCH, Weinheim (Germany), **2003**.
[21] T. Schrader, A. D. Hamilton, *Functional Synthetic Receptors*, Wiley-VCH, Weinheim (Germany), **2005**.
[22] K. Heinze, M. Schlenker, *Eur. J. Inorg. Chem.* **2004**, 2974–2988.
[23] K. Heinze, M. Schlenker, *Eur. J. Inorg. Chem.* **2005**, 66–71.
[24] K. Heinze, M. Beckmann, *Eur. J. Inorg. Chem.* **2005**, 3450–3457.
[25] T. Okamura, T. Iwamura, S. Seno, H. Yamamoto, N. Ueyama, *J. Am. Chem. Soc.* **2004**, *126*, 15972–15973.
[26] D. R. van Staveren, N. Metzler-Nolte, *Chem. Rev.* **2004**, *104*, 5931–5985.
[27] A. Maurer, H.-B. Kraatz, N. Metzler-Nolte, *Eur. J. Inorg. Chem.* **2005**, 3207–3210.
[28] F. Noor, A. Wüstholz, R. Kinscherf, N. Metzler-Nolte, *Angew. Chem.* **2005**, *117*, 2481–2485; *Angew. Chem. Int. Ed.* **2005**, *44*, 2429–2432.
[29] Y.-T. Long, E. Abu-Irhayem, H.-B. Kraatz, *Chem. Eur. J.* **2005**, *11*, 5186–5194.
[30] G. A. Orlowski, S. Chowhury, Y.-T. Long, T. C. Sutherland, H.-B. Kraatz, *Chem. Commun.* **2005**, 1330–1332.
[31] X.-J. Yang, F. Drepper, B. Wu, W.-H. Sun, W. Haehnel, C. Janiak, *Dalton Trans.* **2005**, 256–267.
[32] *Fmoc Solid Phase Peptide Synthesis* (Eds.: W. C. Chan, P. D. White), Oxford University Press, Oxford, **2000**.
[33] R.-A. Fallahpour, *Synthesis* **2000**, *8*, 1138–1142.
[34] R.-A. Fallahpour, *Eur. J. Inorg. Chem.* **1998**, 1205–1207.
[35] R.-A. Fallahpour, M. Neuburger, M. Zehnder, *New J. Chem.* **1999**, *23*, 53–61.
[36] R. Schwesinger, C. Hasenfratz, H. Schlemper, L. Walz, E. M. Peters, K. Peters, H. G. von Schnering, *Angew. Chem.* **1993**, *105*, 1420–1422; *Angew. Chem. Int. Ed. Engl.* **1993**, *32*, 1361–1363.

  

[37] R. Schwesinger, *Nachr. Chem. Tech. Lab.* **1990**, *38*, 1214–1226.
[38] C. Palomo, A. L. Palomo, F. Palomo, A. Mielgo, *Org. Lett.* **2002**, *4*, 4005–4008.
[39] H.-B. Kraatz, J. Lusztyk, G. D. Enright, *Inorg. Chem.* **1997**, *36*, 2400–2405.
[40] M. Duati, S. Tasca, F. C. Lynch, H. Bohlen, J. G. Vos, S. Stagni, M. D. Ward, *Inorg. Chem.* **2003**, *42*, 8377–8384.
[41] Band profiles were fitted using pseudo-Voigt functions (weighted Lorentz/Gauss band profiles) given by the equation: $y = y_0 + A[\mu(2/\pi)\{\omega/[4(x - x_c)^2 + \omega^2]\} + (1 - \mu)\{\sqrt{[4\ln(2)]}/[\sqrt{(\pi)}\omega]\}\exp\{-[4\ln(2)/\omega^2](x - x_c)^2\}]$ using Origin® V 7.0303.
[42] K. Hutchison, J. C. Morris, T. A. Nile, J. L. Walsh, D. W. Thompson, J. D. Peterson, J. R. Schoonover, *Inorg. Chem.* **1999**, *38*, 2516–2523.
[43] T.-Y. Dong, M.-C. Lin, M. Y.-N. Chiang, J.-Y. Wu, *Organometallics* **2004**, *23*, 3921–3930.
[44] Z. Murtaza, D. K. Graff, A. P. Zipp, L. A. Worl, W. E. Jones, W. D. Bates, T. J. Meyer, *J. Phys. Chem.* **1994**, *98*, 10504–10513.
[45] Recently a luminescent complex $[Ru(tpy)(tpy\text{-}COOEt)](PF_6)_2$ with $\Phi = 2.7 \times 10^{-4}$ has been incorporated in a light-emitting electrochemical cell: H. J. Bolink, L. Cappelli, E. Coronado, P. Gaviña, *Inorg. Chem.* **2005**, *44*, 5966–5968.
[46] J.-C. Chambron, C. Coudret, J.-P. Sauvage, *New J. Chem.* **1992**, *16*, 361–367.
[47] E. J. Lee, M. S. Wrighton, *J. Am. Chem. Soc.* **1991**, *113*, 8562–8564.
[48] M. Furue, M. Ishibashi, A. Satoh, T. Oguni, K. Mauyama, K. Sumi, M. Kamachi, *Coord. Chem. Rev.* **2000**, *208*, 103–113.
[49] E. C. Constable, R. W. Handel, C. E. Housecroft, A. F. Morales, B. Ventura, L. Flamigni, F. Barigelletti, *Chem. Eur. J.* **2005**, *11*, 4024–4034.
[50] M. W. Cooke, G. S. Hanan, F. Loiseau, S. Campagna, M. Watanabe, Y. Tanaka, *Angew. Chem.* **2005**, *117*, 4959–4962; *Angew. Chem. Int. Ed.* **2005**, *44*, 4881–4884.
[51] M. J. Frisch, G. W. Trucks, H. B. Schlegel, G. E. Scuseria, M. A. Robb, J. R. Cheeseman, J. A. Montgomery Jr, T. Vreven, K. N. Kudin, J. C. Burant, J. M. Millam, S. S. Iyengar, J. Tomasi, V. Barone, B. Mennucci, M. Cossi, G. Scalmani, N. Rega, G. A. Petersson, H. Nakatsuji, M. Hada, M. Ehara, K. Toyota, R. Fukuda, J. Hasegawa, M. Ishida, T. Nakajima, Y. Honda, O. Kitao, H. Nakai, M. Klene, X. Li, J. E. Knox, H. P. Hratchian, J. B. Cross, C. Adamo, J. Jaramillo, R. Gomperts, R. E. Stratmann, O. Yazyev, A. J. Austin, R. Cammi, C. Pomelli, J. W. Ochterski, P. Y. Ayala, K. Morokuma, G. A. Voth, P. Salvador, J. J. Dannenberg, V. G. Zakrzewski, S. Dapprich, A. D. Daniels, M. C. Strain, O. Farkas, D. K. Malick, A. D. Rabuck, K. Raghavachari, J. B. Foresman, J. V. Ortiz, Q. Cui, A. G. Baboul, S. Clifford, J. Cioslowski, B. B. Stefanov, G. Liu, A. Liashenko, P. Piskorz, I. Komaromi, R. L. Martin, D. J. Fox, T. Keith, M. A. Al-Laham, C. Y. Peng, A. Nanayakkara, M. Challacombe, P. M. W. Gill, B. Johnson, W. Chen, M. W. Wong, C. Gonzalez, J. A. Pople, *Gaussian 03*, Revision B.03, Gaussian, Inc., Pittsburgh, PA, **2003**.
[52] R. Hooft, Collect, Data Collection Software, Nonius, The Netherlands, **1998**; http://www.nonius.com.
[53] G. M. Sheldrick, *SHELXS-97, Program for Crystal Structure Solution*, University of Göttingen, Germany, **1997**; G. M. Sheldrick, *SHELXL-97, Program for Crystal Structure Refinement*, University of Göttingen, Germany, **1997**; http://www.shelx.uni-ac.gwdg.de/shelx/index.html; *International Tables for X-ray Crystallography*, Kynoch Press, Birmingham, UK, **1974**, vol. 4.
[54] L. Zsolnai, G. Huttner, *XPMA*, University of Heidelberg, Germany, **1998**; http://www.rzuser.uni-heidelberg.de/~il1/laszlo/xpm.html.
[55] R. Soltek, G. Huttner, *WinRay*, University of Heidelberg, Germany, **1999**; http://www.uni-heidelberg.de/institute/fak12/AC/huttner/frame/frame_soft.html.

Received: December 2, 2005
Published Online: March 22, 2006

  